Energy Reports 8 (2022) 11271–11287

Contents lists available at ScienceDirect

Energy Reports

journal homepage: www.elsevier.com/locate/egyr

Research paper

An evaluation method of distributed generation credible capacity based on island partition

Chen Jiahao [a], Sun Bing [a,*], Li Yunfei [a], Jing Ruipeng [a], Zeng Yuan [a], Li Minghao [b]

[a] Key Laboratory of Smart Grid of Ministry of Education, Tianjin University, Tianjin, China
[b] State Grid Tianjin Electric Power Co., Ltd., Tianjin, China

ARTICLE INFO

Article history:
Received 3 April 2022
Received in revised form 15 August 2022
Accepted 27 August 2022
Available online 9 September 2022

Keywords:
Island partition model
Distributed generation credible capacity
Hypothesis test
Equal power supply reliability criterion
Sequential Monte Carlo simulation
Prospective greedy algorithm

ABSTRACT

Distributed generation (DG) has not only electricity value, but also capacity value. The capacity value can be represented by the credible capacity (CC) based on the equal power supply reliability criterion. The evaluation of reliability on distribution network (DN) is the core of CC calculation. Under a fault state, DGs can continue to supply power to some load by the island operating mode, and the DN reliability can be improved. Therefore, it is necessary to utilize the power supply restoration potential of DG and formulate an island partition scheme accurately in the reliability calculation of DN. A DG CC evaluation method based on island partition is proposed in the paper. The power supply reliability of an active distribution network is evaluated based on an island partition model, to realize the accurate evaluation of DG CC. The main work is as follows: First, an island partition model under a random fault state of DN is established. The fluctuation of DGs and load, interconnection switch, load priority, secondary outage constraint and other factors are fully considered in reliability assessment. A heuristic prospective greedy algorithm and the Prim algorithm are used to solve the island partition model accurately. Second, a reliability evaluation method of DN based on sequential Monte Carlo simulation (SMCS) is proposed. The system reliability level can be accurately analyzed under a fault state. Then, a CC evaluation method based on hypothesis testing is proposed. The convergence of the CC searching process can be scientifically judged by checking the conspicuousness of the reliability indices distribution obtained by the SMCS. Finally, a case study of the PG&E 69-bus system is analyzed. The topology of the DN, permeability of the DG and island partition strategy are known to have a significant impact on the DG CC.

1. Introduction

Renewable energy power generation will play a central role in reducing greenhouse gas emissions and achieving the Chinese goal of carbon emissions peak before 2030 and carbon neutralization before 2060 (Zhao et al., 2021). Distributed generation (DG) has not only electricity value, but also capacity value (Sun et al., 2022). The scientific capacity value evaluation results can avoid the redundant configuration of equipment in power system planning (Sun et al., 2021). Renewable energy generation can be guided to improve reliability during the peak period of system load (Fang et al., 2021). Therefore, research to quantify the capacity value of variable renewable power generation is both useful and urgent (Sun et al., 2017).

Renewable energy generation has the characteristics of variability, uncertainty and spatial diversity. Therefore, the contribution of renewable energy generation with the same capacity for system reliability is different from that the contribution of conventional units. Estimating the capacity value of renewable energy accurately is challenging (Zhou et al., 2018). Through the research of domestic and foreign scholars, measuring the capacity value with CC is a mature method for renewable energy generation. It is often broadly defined as the share of a generator nameplate capacity that can be relied on during critical peak moments (Madaeni et al., 2012). The method of definition of CC generally includes equivalent load carrying capacity (ELCC), equivalent firm capacity (EFC), equivalent conventional power plant, and guaranteed capacity (Zhou et al., 2016). Due to the better universality and comparability of CC calculation results, the definition method of EFC and ELCC are used in most of the research. In contrast, EFC defines CC under an equal load demand level, which is applicable to the comparison between multiple power planning schemes in a year. ELCC defines CC under equal capacity of conventional unit, which is applicable to the comparison under different renewable energy permeability schemes (Zhang et al., 2015). The study on the ELCC of generating units was first carried out by Garver in 1966 (Zhao et al., 2019a).

* Corresponding author.
E-mail address: sunbing@tju.edu.cn (B. Sun).

https://doi.org/10.1016/j.egyr.2022.08.251

Nomenclature

Abbreviations

CC	Credible capacity
DG	Distributed generation
DN	Distribution network
EENS	Expected energy not served
EFC	Equivalent firm capacity
ELCC	Equivalent load carrying capacity
IEEE	Institute of Electrical and Electronics Engineers
KP	Knapsack problem
PV	Photovoltaic
SMCS	Sequential Monte Carlo simulation

μ_i	The mean values of population X_i
ω_{ij}	Variable set to 1 if the line between node i and node j is connected and to 0 if the line is disconnected
β_{ij}	Variable set to 1 if node i is the parent of node j and to 0 otherwise.
λ_k	The failure rate of the k_{th} component
γ_k	The repair rate of the k_{th} component
$\boldsymbol{\Omega}^{\text{DG}}$	The set of DG integration nodes
$\boldsymbol{\Omega}_a^{\text{DG}}$	The set of DG integration nodes in the a_{th} island
$\boldsymbol{\Omega}_a^{\text{load}}$	The set of load nodes in the a_{th} island
A	The number of islands in DN
$B_{i,t}$	The benefit value of node i at time t
B_V	The total load benefits in set $\boldsymbol{V}$
$B_V(i)$	The benefit value of node i in set $\boldsymbol{V}$
C_{r}	The installed capacity of conventional units
C_{W}	The installed capacity of wind turbine
C_{PV}	The installed capacity of PV
C_{R}	The remaining electricity of DG
C_{G}	The maximum capacity of superior gird
$\boldsymbol{E}$	The branch set storing all branches information in Prim searching
E'	The updating branch set
E_{NS}	The EENS index under fault state during the evaluation period T
f	Function of reliability level
$\boldsymbol{G}$	The updated undirected graph of distribution network
$\boldsymbol{G}'$	The original undirected graph of distribution network
$G_{i,t}$	DG power output of node i at time t
$G_{i,t}^{\max}$	The maximum DG power output of node i at time t
$I_{ij,t}$	The branch current of the line between node i and node j at time t
$I_{ij}^{\max}$	The upper current limit of branch between node i and node j
L	The load level of system
ΔL	The increased load level
M	The number of DGs
N	The number of load nodes in DN
$\boldsymbol{NE}^1$	The neighborhood nodes set of set $\boldsymbol{V}$
N_0	The number of nodes in $\boldsymbol{NE}^1$
$\boldsymbol{NB_i}$	The neighborhood nodes set of node i
$NE^1(m)$	The m_{th} node in $\boldsymbol{NE}^1$
$\boldsymbol{NE}_m^2$	The neighborhood nodes set of the m_{th} node $NE^1(m)$ in $\boldsymbol{NE}^1$
$NE_m^2(n)$	The n_{th} neighborhood node of $NE^1(m)$
N_m	The number of nodes in $\boldsymbol{NE}_m^2$
n_i	Sampling times of population X_i
$P_{i,t}$	The active power of node i at time t
$P_V(i)$	The active power of node i in set $\boldsymbol{V}$
PR_i	The priority of load node i
P_V	The total active power of all nodes in set $\boldsymbol{V}$
r	A random number obeying 0–1 distribution
r_{m}	The marginal CC rate of lastly integrated DG
r_{c1}	The CC rate when the total capacity of DG is $C1$
r_{c}	The CC rate
S_i^2	The variance of population X_i
S_{E}	Average service availability index
ST_i	A 0–1 variable denoting whether node i can be restored under fault state
$st_{i,t}$	A 0–1 variable denoting whether node i can be restored at time t
s_a	The compressed node of the a_{th} island
$\boldsymbol{SQ}_k$	The sequence operation state vector of the k_{th} component
t_1	The initial time of the fault
t_2	The end time of the fault
T	The evaluation period
t_k^{F}	The normal operation time of the k_{th} component
t_k^{R}	The fault duration time of the k_{th} component
$t_{k,j}^{\text{F}}$	The normal operation time of the k_{th} component under the j_{th} sampling
$t_{k,j}^{\text{R}}$	The fault duration time of the k_{th} component under the j_{th} sampling
$U_{i,t}$	The voltage of node i at time t
$U_t^{\min}$	The lower limit of the node voltage at time t
$U_t^{\max}$	The upper limit of the node voltage at time t
$\boldsymbol{V}$	The set of load nodes drawn into the island
$Va^1(m)$	The value ratio of node $NE^1(m)$
$Va_m(n)$	The combination value ratio of neighborhood node $NE^1(m)$ and prospective neighborhood node $NE_m^2(n)$
$Va_{\max}$	The optimal value ratio
$\boldsymbol{W}$	The node set storing all nodes information in Prim searching
W'	The updating node set
X_i	The population of i_{th} reliability level
$\overline{X_i}$	The mean values of population X_i

The definition of ELCC can be broadly expressed as the amount of additional load from an increase in renewable energy generation capacity while maintaining an equal power supply reliability criterion (Paik et al., 2021). Accurate calculation of the ELCC requires a large amount of data, such as the installed capacity, load demand and failure rate of the component. Despite the huge computational complexity and data demand, CC evaluation based on the ELCC concept is one of the most accurate and theoretically reliable methods. In the context of the paper, the CC of renewable

energy is the ELCC or the ratio of ELCC to the nameplate capacity of renewable energy generation.

A large number of studies have been carried out by many scholars to evaluate the CC of wind turbine and photovoltaic (PV) equipment. However, the existing research focuses mainly on centralized renewable energy stations, which are connected to power generation and transmission systems. However, there are great differences in network topology and operation mode between transmission and distribution systems. Therefore, the CC evaluation method of centralized renewable energy stations cannot be used directly in DG CC evaluation (Ochoa et al., 2010).

The DG CC calculation method considering system reliability generally includes the following four links: modeling of renewable energy output, selection of reliability indices, calculation of system reliability and searching of CC value (Zhang et al., 2015). The output of renewable energy power generation is greatly affected by meteorological factors such as wind speed and solar radiation intensity. Therefore, the accurate construction of the output model is significant for CC evaluation. The existing models are divided into two categories according to whether the sequential output of renewable energy power generation is considered. The multistate unit model (Chen et al., 2019) and output probability model (Wang et al., 2019) are models that do not consider sequential output. Due to ignoring the output sequence and the correlation between power generation and demand, there is a large deviation between the CC evaluation result and the real value. In contrast, the sequential output modeling method requires strict sequential characteristic information and the calculation process is complex. However, the daily fluctuation and seasonal variation of output can be considered effectively in sequential output modeling and it is a more accurate scheme for renewable energy modeling.

In the CC search process, the system reliability indices need to be calculated repeatedly until the equal reliability criterion is met. The CC search process is essentially a one-dimensional search process. The dichotomy and secant method (Cai and Xu, 2021) are effective methods to obtain the CC value, which can generally meet the calculation requirements. For the selection of convergence conditions, the existing research usually selects a minimum value as the convergence criteria. However, the reliability calculation results based on the SMCS method have random errors, and the reliability indices are not absolutely accurate. The CC calculation results may deviate greatly if the value of artificially selected convergence criteria is large. Meanwhile, if the accuracy of the convergence criteria is strict, the iteration may repeat in the neighborhood of the convergence value, which leads to the difficulty of convergence and takes up considerable computing time.

The DG is integrated into medium and low voltage DN and consumed nearby. With the characteristics of large quantity and scattered distribution, reliability evaluation with DG is difficult. In reliability calculations, the selection of the reliability indices has an important impact on CC evaluation results (Wilton et al., 2014). Loss of energy expected (Shahidirad et al., 2018; Miao et al., 2018) and expected energy not served (EENS) (Zhang et al., 2021; Li et al., 2018) are usually selected as reliability indices in most references. There are abundant studies on the reliability evaluation of DNs. Ref. Luo et al. (2021) explores the DN reliability improvement method considering the demand side response for the construction of an integrated energy system. Ref. Li et al. (2016) evaluates DN reliability based on user satisfaction. The reference integrates reliability and operation economy to ensure that the DN operates at the maximum benefit point. However, the above references do not consider the effect of DG on the reliability during island operation mode. The island partition scheme must be formulated to fully utilize the power supply restoration potential of DG under a fault state.

Island partition modeling is the core work in the process of DN reliability evaluation based on island partition. Based on historical data, Ref. Zhao et al. (2019b) generates DG scenarios and their probability distributions according to the sequence characteristics and uncertainty output of DG. The island partition model of an active distribution network with restoration load as the objective function is established. However, the effect of load priority on the power supply restoration sequence is not considered. Ref. Hosseinnezhad et al. (2018) establishes the island model of an intelligent distribution network based on a severe disturbance environment by integrating the constraints of load demand and priority. However, the expansion path of power supply recovery by interconnection switch is ignored. Therefore, the effect of various constraints should be considered comprehensively on island partition modeling to maximize the benefit of load recovery under island mode.

The existing methods for solving the island partition model can be divided into the graph theory partition method (Slota et al., 2020), tree knapsack method (Oboudi et al., 2017) and heuristic algorithm (Wen et al., 2021; Wu et al., 2015). Among these methods, the graph theory partition method essentially transforms the island partition problem into the minimum spanning tree problem. The minimum spanning tree problem can be well solved based on the Prim algorithm (Ahangar et al., 2020). Through the tree knapsack method, the optimal island partition problem can be transformed into a tree knapsack problem. Then, the problem of DG island partition is solved based on the strategy of search and adjustment. However, the graph theory partition problem and tree knapsack problem are typical NP hard problems and the proposed methods cannot reconcile calculation speed and accuracy. In addition, most studies on island partition formulate schemes only within a certain time period. The fluctuation of DGs and load demand is not considered comprehensively and island partition is not applied to the sequential reliability calculation of the DN.

Moreover, the approximate calculation method of CC without reliability evaluation is introduced in some references. The CC approximation method based on the capacity factor is proposed in Ref. Bethany et al. (2017). To weigh the cost and value of all power generation resources, the marginal CC rate of renewable energy is updated dynamically over DG permeability and system configuration investment. An analytical probability method for evaluating the reliability of long-term planning based on the Z-method is mentioned in Ref. Aghaei et al. (2013). The method can quickly and effectively evaluate the system reliability and guide the formulation of an optimal investment scheme for renewable energy. An analytical method for DN reliability evaluation is proposed in Ref. Voorspools and d'Haeseleer (2006). In this method, DN reconfiguration and DG scheduling are fully considered, and the robustness of the DN is improved. A reliability analysis and calculation method based on influence increment is proposed in Ref. Ryan et al. (2016), and the evaluation of generation efficiency and transmission reliability is decoupled. The above method can effectively reduce the calculation time in the process of reliability evaluation, and the factors affecting CC can be revealed more intuitively. The above methods generally set strong assumptions, and they can be applied in some specific occasions. In addition, some studies have explored the CC value under different scenarios, such as microgrid (Costa and Matos, 2010; Rajam, 2020), micro-heat cogeneration (Hawkes and Leach, 2008; Remiorz et al., 2018), energy storage (Amelin, 2009; Salama et al., 2021) and demand side response (Zeng et al., 2018; Lynch et al., 2019). However, CC evaluation methods between different scenarios are not universal.

Throughout the research on the calculation method of DG CC, the following shortcomings can be found in the existing

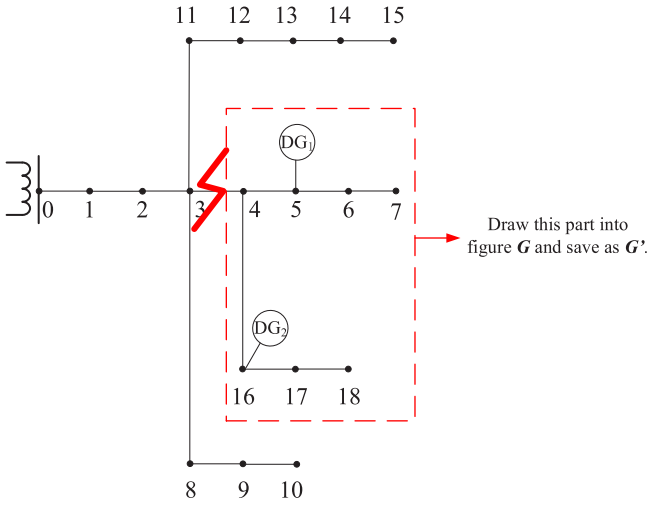

Fig. 1. The range of $\boldsymbol{G}$ to be restored.

research: (1) Aiming at island partition under fault state, the existing research did not fully consider important factors such as interconnection switch, load priority and secondary outage constraint in modeling. There is still no research taking island partition into the DG CC evaluation. (2) Usually, a small constant value is used as the convergence criteria of CC searching. When a subjective number is selected, CC calculation results may deviate from the true value, or the calculation process oscillates in the neighborhood of the true value.

To solve the above problems, a DG CC evaluation method based on island partition is proposed in the paper. The characteristic is that the island partition is firstly used in CC evaluation as the reliability calculation method. The island partition scheme can be formulated quickly based on the prospective greedy algorithm and Prim algorithm. And the equal power supply reliability criterion is realized based on hypothesis testing method. The method overcomes the convergence difficulty caused by artificially selecting the minimum value as the convergence criteria. Finally, the effectiveness of the proposed method is verified by a case study, and the key factors affecting DG CC are analyzed. The permeability of DG and secondary outage constraint have a significant impact on CC evaluation results. However, the failure rate of the component, uniformity of the load node and DG integration location have little impact on the DG CC.

2. Reliability calculation and island partition optimization model

2.1. Island partition

2.1.1. Island partition optimization model

The DN usually operates radially. The power supply reliability of the system may be affected when the components are under fault state. The load downstream of the fault component cannot obtain electricity from the superior power grid. The topology of DN can be changed flexibly. The scientific island partition scheme can be formulated to fully utilize the power supply restoration potential of DG under fault state. If the system operates under fault state at time t, the superior grid can be equivalent to a DG with output no more than C_{G} and continue to supply power to the load together with other DGs. The necessary condition for a load node to be restored is that at least one of all nodes directly connected to it has already been restored. When the electricity of each DG cannot meet the power demand of the surrounding load, the power supply recovery process ends and the island partition scheme at time t is obtained. The recovery strategy of the system load under fault state is required to consider the secondary outage constraint. That is, the final island partition scheme under a continuous fault state is the intersection of island partition schemes at each moment. The load nodes that can be recovered at all moments are drawn into an island.

For the DN with N load nodes and M DGs, the island partition scheme can be modeled as a knapsack problem (KP). The active power of each node can be regarded as the weight of the item. The active output of DG can be regarded as the backpack capacity. The product of the active power of the knapsack node and corresponding load weight is regarded as benefit B, and the value B is selected as the objective function. Then, for the k_{th} fault, the knapsack model of the island partition is as follows:

$$\min \sum_{t=t_1}^{t_2} \sum_{a=1}^{A} \sum_{i \in \boldsymbol{\Omega}_a^{\mathrm{load}}} B_{i,t} * (1 - ST_i),$$

$$s.t. \begin{cases} \sum\limits_{i \in \boldsymbol{\Omega}_a^{\mathrm{load}}} P_{i,t} * st_{i,t} = \sum\limits_{j \in \boldsymbol{\Omega}_a^{\mathrm{DG}}} G_{j,t} \quad \forall a \in [1, A] \\ G_{j,t} \le G_{j,t}^{\max} \qquad \forall j \in \boldsymbol{\Omega}_a^{\mathrm{DG}} \quad \forall t \in [t_1, t_2] \\ B_{i,t} = P_{i,t} * PR_i \\ \boldsymbol{\Omega}_a^{\mathrm{load}} \cap \boldsymbol{\Omega}_b^{\mathrm{load}} = \varnothing \quad \forall a \in [1, A], b \in [1, A], a \ne b \\ \boldsymbol{\Omega}_a^{\mathrm{DG}} \cap \boldsymbol{\Omega}_b^{\mathrm{DG}} = \varnothing \quad \forall a \in [1, A], b \in [1, A], a \ne b \\ st_{i,t} = \begin{cases} 1 & if\ i \in \bigcup\limits_{a=1}^{A} \boldsymbol{\Omega}_a^{\mathrm{load}} \\ 0 & else \end{cases} \\ ST_i = \begin{cases} 1 & if\ st_{i,t} = 1 \forall t \in [t_1, t_2] \\ 0 & else \end{cases} \\ U_t^{\min} * st_{i,t} \le U_{i,t} \le U_t^{\max} * st_{i,t} \\ I_{ij,t} \le I_{ij,t}^{\max} \\ \beta_{ij} + \beta_{ji} = \omega_{ij} \quad \forall i \in \boldsymbol{\Omega}_a^{\mathrm{load}}, j \in \boldsymbol{NB_i}, \forall a \in [1, A] \\ \beta_{ij} = 0 \qquad \forall i \in \boldsymbol{\Omega}_a^{\mathrm{DG}}, \forall a \in [1, A] \\ \beta_{ij} \in \{0, 1\} \qquad \forall i \in \boldsymbol{\Omega}_a^{\mathrm{load}}, \forall i \notin \boldsymbol{\Omega}_a^{\mathrm{DG}}, j \in \boldsymbol{NB_i}, \forall a \in [1, A] \\ 0 \le \omega_{ij} \le 1 \qquad \forall i \in \boldsymbol{\Omega}_a^{\mathrm{load}}, j \in \boldsymbol{NB_i}, \forall a \in [1, A] \\ \sum\limits_{j \in \boldsymbol{NB_i}} \beta_{ij} = 1 \quad \forall i \in \boldsymbol{\Omega}_a^{\mathrm{load}}, \forall i \notin \boldsymbol{\Omega}_a^{\mathrm{DG}}, \forall a \in [1, A] \end{cases} \tag{1}$$

2.1.2. Prospective greedy algorithm

The island partition model established in Section 2.1.1 is a 0–1 mixed integer nonlinear programming model, which is complex and difficult to solve. A heuristic prospective greedy algorithm is used to formulate the island partition scheme. The algorithm can effectively overcome the blindness of single-step selection of the existing methods, bring greater benefits and reduce the outage loss to a greater extent. The steps of the prospective greedy algorithm under fault state at time t can be listed as follows:

(1) Update the topology of DN according to the location of fault components at time t. The loads that lose connection with the superior power grid are drawn into figure $\boldsymbol{G}$. Save a copy of figure $\boldsymbol{G}'$. For example, the line between node 3 and node 4 fails as shown in Fig. 1. The downstream load cannot be supplied by the superior grid under fault state.

(2) Determine the power supply order of the DG and formulate the restoration scheme of each DG at time t in turn.

① Select the DG with the largest capacity that is not marked, and select the integration node as the KP initial node. Judge

whether the electricity of the DG is greater than the active power of the integration node. If yes, update the remaining electricity of DG by subtracting the load demand of nodes. If not, mark the DG and repeat step ①.

② The total active power of all nodes in set $\boldsymbol{V}$ is denoted as P_V, the sum of benefit is recorded as B_V, and the remaining electricity of DG is denoted as C_{R}. Update P_V, B_V and C_{R} of set $\boldsymbol{V}$ according to Eqs. (2)–(4):

$$P_V = \sum_{i \in \boldsymbol{V}} P_{i,t} \tag{2}$$

$$B_V = \sum_{i \in \boldsymbol{V}} P_{i,t} * PR_i \tag{3}$$

$$C_{\mathrm{R}} = \sum_{i \in \boldsymbol{V} \cap \boldsymbol{\Omega}^{\mathrm{DG}}} G_{i,t} - P_V \tag{4}$$

③ Search the neighborhood set $\boldsymbol{NE}^1$ and prospective neighborhood $\boldsymbol{NE}_m^2$ of $\boldsymbol{V}$

Search for nodes that are directly connected to the nodes in $\boldsymbol{V}$ but do not belong to set $\boldsymbol{V}$. The set composed of such nodes is named the neighborhood set of $\boldsymbol{V}$. The set is denoted as $\boldsymbol{NE}^1$, and the number of nodes in $\boldsymbol{NE}^1$ is denoted as N_0. For the m_{th} node $NE^1(m)$ in set $\boldsymbol{NE}^1$, $m \in \{1, 2,\ldots, N_0\}$, search for nodes directly connected to $NE^1(m)$ but not belonging to sets $\boldsymbol{V}$ and $\boldsymbol{NE}^1$. The set composed of such nodes is named the prospective neighborhood of $\boldsymbol{V}$. The set is denoted as $\boldsymbol{NE}_m^2$, and the number of nodes in $\boldsymbol{NE}_m^2$ is denoted as N_m. Where, $NE_m^2(n)$ denotes the n_{th} neighborhood node of $NE^1(m)$, $m \in \{1, 2,\ldots, N_0\}$, and $n \in \{1, 2,\ldots, N_m\}$.

④ Calculate the value ratio corresponding to each neighborhood node

The value ratio $Va^1(m)$ of node $NE^1(m)$ is calculated as follows:

$$Va^1(m) = \begin{cases} \frac{B_V(NE^1(m))}{P_V(NE^1(m))}, & if\ P_V(NE^1(m)) \le C_{\mathrm{R}} \\ 0, & if\ P_V(NE^1(m)) > C_{\mathrm{R}} \end{cases} \tag{5}$$

The value ratio $Va_m(n)$ of the combination of neighborhood node $NE^1(m)$ and prospective neighborhood node $NE_m^2(n)$ is calculated as follows:

$$Va_m(n) = \begin{cases} \frac{B_V(NE^1(m)) + B_V(NE_m^2(n))}{P_V(NE^1(m)) + P_V(NE_m^2(n))}, & if\ P_V(NE^1(m)) + P_V(NE_m^2(n)) \le C_{\mathrm{R}} \\ 0, & if\ P_V(NE^1(m)) + P_V(NE_m^2(n)) > C_{\mathrm{R}} \end{cases} \tag{6}$$

⑤ Calculate the optimal value ratio $Va_{\max}$ corresponding to neighborhood set $\boldsymbol{NE}^1$ and prospective neighborhood set $\boldsymbol{NE}_m^2$ of $\boldsymbol{V}$

$$Va_{\max} = \max\{Va^1(m), Va_m(n)\} \quad \forall m \in \{1, 2, \ldots, N_0\},\ n \in \{1, 2, \ldots, N_m\} \tag{7}$$

If $Va_{\max}$ is 0, mark the DG and exit the iterative calculation. Set $\boldsymbol{V}$ is the load node corresponding to the current DG that can be recovered. If $Va_{\max}$ is not 0, the node corresponding to the maximum value is drawn into the set $\boldsymbol{V}$. Then, return to step ②. If the value ratio is the same, the nodes with a large active load shall be preferentially drawn into the island.

(3) Compress all the nodes obtained in step (2) into new nodes s_a

For all nodes in $\boldsymbol{\Omega}_a^{\mathrm{load}}$, check whether there is a connection relationship between them. If yes, disconnect the line and compress the scattered nodes into a new node s_a. If the node in $\boldsymbol{\Omega}_a^{\mathrm{load}}$ has a connection relationship with the external node of $\boldsymbol{\Omega}_a^{\mathrm{load}}$, s_a will maintain the connection relationship with the external node. Check whether there are multiple nodes in $\boldsymbol{\Omega}_a^{\mathrm{DG}}$. If yes, the multiple DGs integrated into the corresponding nodes are merged into a new DG and the new DG is integrated into the compression node s_a. The output is the sum of the C_{R} of each DG before merging.

(4) Check whether there are unmarked DGs in figure $\boldsymbol{G}$. If yes, go to step (2). Otherwise, go to step (5).

(5) Each compression node s_a denotes an island. Restore s_a to the original node and determine the island partition scheme according to $\boldsymbol{G}'$.

(6) There are interconnection switches in the DN, and the island partition scheme obtained by the prospective greedy algorithm may have a ring network. The Prim algorithm of the minimum spanning tree is applied to transform the ring network into a radial structure.

(7) Check the node voltage and power flow constraints. Change the island partition scheme according to the power flow calculation results until all constraints are met.

2.1.3. Prim algorithm

The Prim algorithm is an algorithm for finding the minimum spanning tree in a weighted undirected graph. For the ring structure of a weighted undirected graph, the Prim algorithm can be used to search an acyclic path containing all nodes and the sum branch weights composed of the path are the lowest. The Prim algorithm is considered to minimize the operation times of the interconnection switch in the process of formulating the island partition and restoring the power supply. When there is a ring network in the island partition scheme, disconnection of the interconnection switch is preferred. According to the above principle, the branch weight of the interconnection switch is set to be greater than the branch weight of the distribution feeder. Then, the Prim algorithm is used to search a power supply path that meets the radial constraint, and the sum branch weights of the path are the lowest. The specific steps of the Prim algorithm are as follows:

(1) According to the existing island partition results, a scheme with a ring network is formed. Set the weight of the distribution feeder to 1 and the weight of the interconnection switch to 2.

(2) Establish node set $\boldsymbol{W}$ and branch set $\boldsymbol{E}$. The two sets store all the node and branch information in the topology respectively. Establish the corresponding sets $\boldsymbol{W}'$ and $\boldsymbol{E}'$. Empty set $\boldsymbol{E}'$. Select one node arbitrarily as the initial node w_0 to start the search. The initial node is drawn into the set $\boldsymbol{W}'$. $\boldsymbol{E}' = \varnothing$, $\boldsymbol{W}' = \{w_0\}$.

(3) Judge whether set W' is the same as set $\boldsymbol{W}$. If yes, go to step (5). Otherwise, go to step (4).

(4) Search for the branch $l_{u,w}$ with the lowest branch weight in set $\boldsymbol{E}$, where u is the node in $\boldsymbol{W}'$, and node w is not in $\boldsymbol{W}'$. Update sets $\boldsymbol{W}'$ and $\boldsymbol{E}'$, incorporate node w into $\boldsymbol{W}'$ and incorporate branches $l_{u,w}$ into set $\boldsymbol{E}'$. If there are multiple branches that meet the above conditions, such as the branch weight being the same, choose one branch at random. Return to step (3) for judgement.

(5) The searching process is stopped, and the obtained sets $\boldsymbol{W}'$ and $\boldsymbol{E}'$ are the nodes and branches contained in the final island partition scheme with a radial network.

Fig. 2 describes the process of solving the minimum spanning tree based on the Prim algorithm. The topology shown in Fig. 2(a) contains a ring network, and nodes A∼F are stored in set $\boldsymbol{W}$. Node A is selected as the initial node and searches the branch with the lowest branch weight. Incorporate branches $l_{\mathrm{A,E}}$ into set $\boldsymbol{E}'$, and node E is drawn into set $\boldsymbol{W}'$. For the second search, the weights of branch $l_{\mathrm{E,F}}$ and branch $l_{\mathrm{E,D}}$ are 2. At this time, the branch $l_{\mathrm{E,F}}$ is selected randomly and drawn into set $\boldsymbol{E}'$. Node F is drawn into set $\boldsymbol{W}'$. The Prim algorithm continues to search until set $\boldsymbol{W}'$ is the same as set $\boldsymbol{W}$, as shown in Fig. 2(e). Then, the final radial topology is obtained.

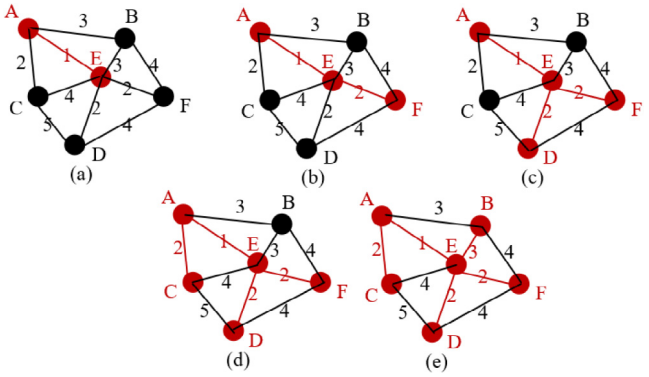

Fig. 2. Searching process of the Prim algorithm.

2.2. Reliability evaluation method based on SMCS

The power supply reliability is closely related to the output of DG and load demand. However, the output of the DG and load demand fluctuate, and the faults of the components in the DN also occur randomly. Therefore, a random sampling method of DG output and system operation state should be carried out in reliability evaluation. The power supply reliability can be evaluated based on SMCS. The main steps are as follows:

(1) Only fault and normal states are assumed to exist in power system operation, and all components operate under a normal state at the beginning of the evaluation period. The failure rate and repair rate of components in a power system obey an exponential distribution. If the k_{th} component is under fault state, the normal operation time t_k^{F} can be generated by random number sampling:

$$t_k^{\text{F}} = -\frac{1}{\lambda_k}\ln r \tag{8}$$

The fault operation time t_k^{R} can be generated in the same way:

$$t_k^{\text{R}} = -\frac{1}{\gamma_k}\ln r \tag{9}$$

(2) Generate the sequence operation state vector of the k_{th} component in the evaluation period T. Continuously calculate t_k^{F} and t_k^{R}, and arrange them by order to obtain the sequence operation state vector $\boldsymbol{SQ}_k$. $\boldsymbol{SQ}_k = \left[t_{k,1}^{\text{F}}, t_{k,1}^{\text{R}}, t_{k,2}^{\text{F}}, t_{k,2}^{\text{R}}, \ldots\ldots\right]$. Repeat step (1) until the following formula is satisfied:

$$T < \sum_j \left(t_{k,j}^{\text{F}} + t_{k,j}^{\text{R}}\right) \tag{10}$$

(3) Let $k = k + 1$, and repeat step (2) to generate the sequence operation state vector of all components. The components to be state sampled include the bus, transformer, distribution feeder, wind turbine and PV equipment. The output is 0 when the DG is under fault state.

(4) For the k_{th} component, judge whether this component is under fault state at time t according to $\boldsymbol{SQ}_k$. If the component is under fault state, go to step (5); otherwise, go to step (6).

(5) Establish and solve the island partition model by the prospective greedy algorithm and Prim algorithm. Calculate the power supply reliability by the island partition scheme at time t.

(6) Let $t = t + 1$, judge whether $t \le T$ is satisfied. If yes, repeat steps (4)–(5) until the end of this component fault analysis. Otherwise, analyze the next fault of the component. Let $t = 1$, $k = k + 1$, return to step (1) until the analysis under all fault conditions is completed.

3. The concept and calculation method of DG CC

In the original system, the installed capacity of conventional units is assumed to be C_{r} and load demand level is L. The power supply reliability level before DG integration is denoted as $f\{C_{\text{r}}, L\}$. After DG is integrated, the power supply reliability can be improved and the load carrying capacity of the system is increased. When the load level of the system reaches $L + \Delta L$, the power supply reliability of the system can be expressed as $f\{C_{\text{r}}+C_{\text{W}}+C_{\text{PV}}, L + \Delta L\}$. If the following formula is satisfied:

$$f\{C_{\text{r}}, L\} = f\{C_{\text{r}} + C_{\text{W}} + C_{\text{PV}}, L + \Delta L\} \tag{11}$$

Under the equal reliability criterion, the CC of DG with an installed capacity of $C_{\text{W}}+C_{\text{PV}}$ is ΔL. The physical meaning of CC can be interpreted as follows: DG can supply additional load on the premise of an equal reliability criterion. To measure the proportion of CC in the DG installed capacity, the concept of CC rate r_{c} is proposed:

$$r_c = \frac{\Delta L}{C_{\text{W}} + C_{\text{PV}}} \times 100\% \tag{12}$$

The value of r_{c} is less than 1. Under the same installed capacity, the higher the value of r_{c} is, the greater the contribution to the power supply reliability.

The CC searching process is the last step of CC calculation and is essentially a one-dimensional searching process. The increased load level ΔL can be obtained by repeated iterative calculation and dichotomy is an effective method to realize a one-dimensional searching process. The steps of the DG CC searching process based on dichotomy are as follows, which can be expressed by Fig. 3.

(1) The yellow solid line in Fig. 3 shows the hypothetical curve of power supply reliability changing with the load level before DG integration. The broken blue line is the hypothetical curve after DG integration. Under the initial condition, the installed capacity of DG is 0, and the reliability level $f\{C_{\text{r}}, L\}$ (as shown in the green level solid line in Fig. 3) is calculated.

(2) Integrate distributed wind turbine with C_{W} capacity and photovoltaic equipment with C_{PV} capacity. The load level remains unchanged at L. Calculate the reliability level $f\{C_{\text{r}}+C_{\text{W}}+C_{\text{PV}}, L\}$ (as shown in the red dot in Fig. 3).

(3) Increase the load level by ΔL_1 and calculate the reliability level f. Judge whether the reliability level f is higher than $f\{C_{\text{r}}, L\}$. If yes, repeat step (3) to increase the load level until the reliability level is lower than $f\{C_{\text{r}}, L\}$. Record the load level L' at this time and calculate the reliability level $f\{C_{\text{r}}+C_{\text{W}}+C_{\text{PV}}, L'\}$ (as shown in the purple dot in Fig. 3).

(4) Adjust the value of ΔL based on the dichotomy in the load level $[L, L']$ interval and calculate reliability level f (as shown in several green dots in Fig. 3). The iteration calculation is repeated until the convergence criteria based on the hypothesis test (such as the blue dot in Fig. 3) is met. The reliability calculation results based on SMCS are random. If a minimum value is artificially selected as the convergence criteria, the number of iterations and convergence accuracy will be greatly affected. Therefore, the equal power supply reliability criterion based on the hypothesis test method is effectively realized in the paper. The calculation speed and accuracy are considered at a given confidence level, and the CC evaluation result is more reliable.

The reliability evaluation results $f\{C_{\text{r}}, L\}$ obtained by SMCS are random. Before DG is integrated, the population of $f\{C_{\text{r}}, L\}$ obtained by SMCS is recorded as X_1. Similarly, the population of $f\{C_{\text{r}}+C_{\text{W}}+C_{\text{PV}}, L'\}$ obtained by SMCS after DG integration is recorded as X_2. μ_1 and μ_2 are the mean values of X_1 and X_2, respectively. For the samples extracted by sampling times n_1 in population X_1, the mean value and variance are $\overline{X}_1$ and S_1^2,

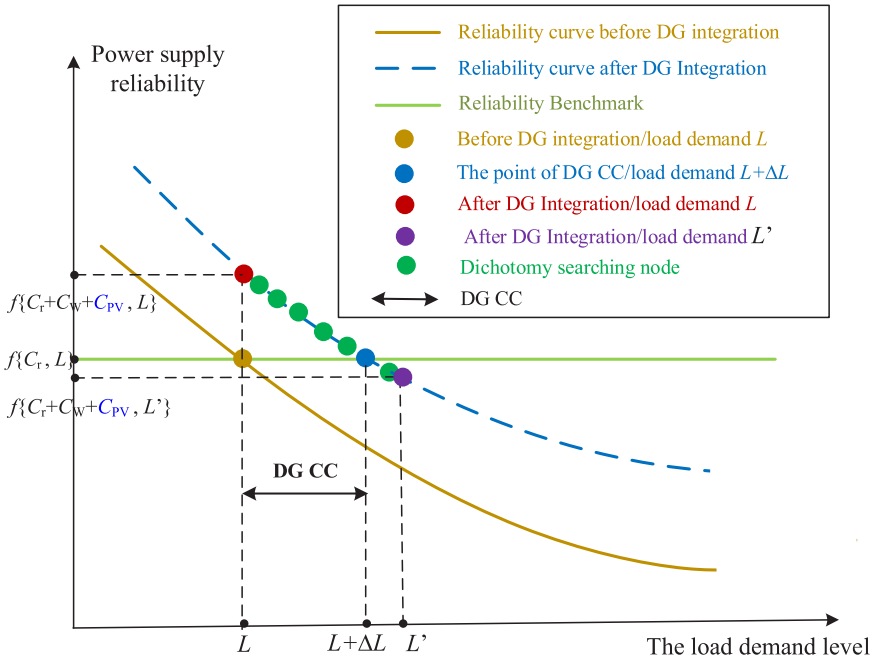

Fig. 3. Schematic diagram of the CC concept. (For interpretation of the references to color in this figure legend, the reader is referred to the web version of this article.)

respectively. For the samples extracted by sampling times n_2 in population X_2, the mean value and variance are $\overline{X}_2$ and S_2^2, respectively. Hypothesis H_0: $\mu_1 = \mu_2$.

When n_1 and n_2 are large enough, the U obtained from the following formula approximately obeys the standard normal distribution:

$$U = \frac{\overline{X}_1 - \overline{X}_2}{\sqrt{\frac{S_1^2}{n_1} + \frac{S_2^2}{n_2}}} \tag{13}$$

Set confidence level α:

$$P\left(\frac{\overline{X}_1 - \overline{X}_2}{\sqrt{\frac{S_1^2}{n_1} + \frac{S_2^2}{n_2}}} \geq \mu_{\frac{\alpha}{2}}\right) \approx \alpha \tag{14}$$

If the following formula is satisfied:

$$\left|\overline{X}_1 - \overline{X}_2\right| \geq \mu_{\frac{\alpha}{2}} * \sqrt{\frac{S_1^2}{n_1} + \frac{S_2^2}{n_2}} \tag{15}$$

H_0 is rejected, and a significant difference between population X_1 and X_2 is considered if the following formula is satisfied:

$$\left|\overline{X}_1 - \overline{X}_2\right| < \mu_{\frac{\alpha}{2}} * \sqrt{\frac{S_1^2}{n_1} + \frac{S_2^2}{n_2}} \tag{16}$$

H_0 is accepted, and no significant difference between the population X_1 and X_2 is considered. The mean value of the extracted samples is regarded as the power supply reliability index.

When the reliability indices are selected differently, the evaluation results of CC will also be different. Analysis of the impact of different reliability indices on CC evaluation results is of great significance. EENS and average service availability index are two important indices of reliability. The calculation method of E_{NS} and average service availability index S_E are calculated as follows:

$$E_{NS} = \sum_{t=1}^{T} \sum_{i \in \boldsymbol{V}} P_{i,t} \tag{17}$$

$$S_E = \frac{\sum_{t=1}^{T} \sum_{i \in \boldsymbol{V}} P_{i,t}}{\sum_{t=1}^{T} \sum_{i=1}^{N} P_{i,t}} \times 100\% \tag{18}$$

The CC can effectively measure the overall capacity value of DG, but it cannot describe the change trend of the capacity value with DG permeability. The concept of the marginal CC rate is proposed to effectively express the dynamic change process of CC with DG increased capacity. The calculation method is as follows:

$$r_m = \frac{r_{c1} - r_{c2}}{C1 - C2} \times 100\% \tag{19}$$

4. Case study

4.1. System parameters

The CC evaluation of DG is carried out for the PG&E 69-bus network. The topology and integration location of DGs are shown in Fig. 4. DG_1 and DG_3 are 1 MW PV, which are integrated into node 5 and 36, respectively. DG_2 and DG_4 are 2 MW wind turbine, which are integrated into node 18 and 52, respectively. Parameters such as the active power and priority of each load can be seen in the appendix. The five interconnection switches are 11–66, 13–21, 15–69, 27–54 and 39–48. The interconnection switches are open under a normal state. The weight of the distribution feeder is 1, and the weight of the interconnection switch is 2. The repair rate of buses, circuit breakers, transformers and other components is 1000 times per year. The superior grid is regarded as an infinite source. The evaluation period T is 10 years.

4.2. Island partition

According to random number sampling results, feeder $l_{0,1}$ breaks down during 2624_{th}–2627_{th} h. The load node of the DN cannot obtain electricity from the superior grid under a fault

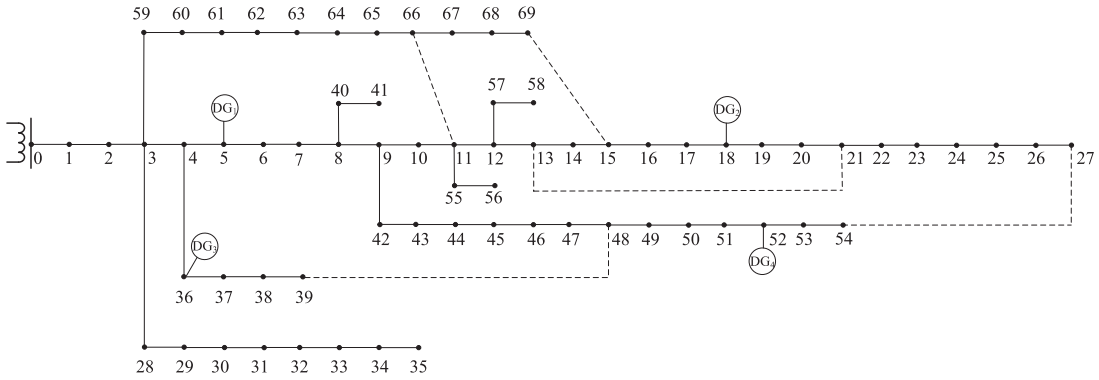

Fig. 4. The topology of the PG&E 69-bus network.

Table 1
Island partition searching process of DG_2.

Step 1: Put node 18 into $\boldsymbol{V}$, search for the next restored node						
Nodes in set V	C_R/kW	$\boldsymbol{NE}^1$ and $\boldsymbol{NE}_m^2$	Load demand/kW	Benefit B_V	$Va^1(m)$ or $Va_m(n)$	Next node drawn into set $\boldsymbol{V}$
18	65.69	17	62.94	62.94	1	19, 20
		17, 16	110.67	540.27	0	
		19, 20	1.05	10.5	10	
Step 2: Put node 18, 19, 20 into $\boldsymbol{V}$, search for the next restored node						
Nodes in set $\boldsymbol{V}$	C_R/kW	$\boldsymbol{NE}^1$ and $\boldsymbol{NE}_m^2$	Load demand/kW	Benefit B_V	$Va^1(m)$ or $Va_m(n)$	Next node drawn into set $\boldsymbol{V}$
18, 19, 20	64.64	21	119.59	1195.90	0	17
		17	62.94	62.94	1	
		21, 22	125.15	1251.52	0	
		21, 13	127.98	1279.80	0	
		17, 16	110.67	540.27	0	
Step 3: Put node 18, 19, 20, 17 into $\boldsymbol{V}$, search for the next restored node						
Nodes in set $\boldsymbol{V}$	C_R/kW	$\boldsymbol{NE}^1$ and $\boldsymbol{NE}_m^2$	Load demand/kW	Benefit B_V	$Va^1(m)$ or $Va_m(n)$	Next node drawn into set $\boldsymbol{V}$
18, 19, 20, 17	1.7	21	119.59	1195.90	0	/
		16	47.74	477.44	0	
		21, 22	125.15	1251.52	0	
		21, 13	127.98	1279.80	0	
		16, 15	47.74	477.44	0	
$Va^1(m)$ and $Va_m(n)$ are zero, and the island searching process of DG_2 ends						

Table 2
Island partition scheme at 2627th hour.

DG number	Initial node	Nodes in set $\boldsymbol{V}$	Load demand/kW	Benefit B	Compression node number
DG_2	18	{17, 18, 19, 20}	126.94	696.86	70
DG_4	52	{52, 51}	33.57	33.34	71
DG_1	5	{1∼15, 21∼23, 28, 36∼37, 40∼47, 55∼57, 63∼69, 70}	1026.92	26 917.98	72

state. The island partition scheme must be formulated for load recovery by DG during 2624_{th}–2627_{th} h. Due to the fluctuation of DG output and load demand, the island partition scheme of each moment is much different from each other. In order to clearly reveal the formulation process of island partition scheme, the island scheme at the moment of 2627_{th} h is introduced in detail. During the island partition scheme formulation, the load recovery is conducted in the order of DG_2, DG_4, DG_1 and DG_3.

Taking the 2627_{th} h as an example, the power recovery scheme of DG_2 is first formulated. The search process of the prospective greedy algorithm is shown in Table 1. Node 18 is drawn into knapsack set $\boldsymbol{V}$, and its neighborhood set includes {17, 19}. The corresponding prospective neighborhood set includes {{17, 16}, {19, 20}}. Calculate the value ratio, select the load node corresponding to the maximum value ratio and put it or them into backpack set $\boldsymbol{V}$. It should be noted that the benefit of {17, 16} is very high, while the value ratio is 0 due to the insufficient remaining DG capacity. When the value ratio of all nodes is 0, the calculation process is stopped. The load node that can be restored by DG_2 at the 2627_{th} h is {17, 18, 19, 20}. The island partition with DG_2 as the initial node is shown in Fig. 5. The load node drawn into the backpack is compressed into s_1, the sum of load demand P_V is 126.94 kW, and the benefit B_V is 703.91. The compressed node is recorded as 70. The s_1 compression diagram is shown in Fig. 6.

Similarly, the power supply restoration scheme is formulated according to the power supply sequence of each DG, and then the island partition scheme at the moment is obtained. The specific process of island partition can be seen in the appendix and is not shown in detail here. The island partition scheme at the 2627_{th} h is shown in Table 2. When all the DGs are marked, the electricity of DGs cannot restore power for the remaining load nodes. That is, the load nodes {16, 24∼27, 29∼35, 38∼39, 48∼50, 53∼54, 58∼62} are out of power at the 2627_{th} h. The

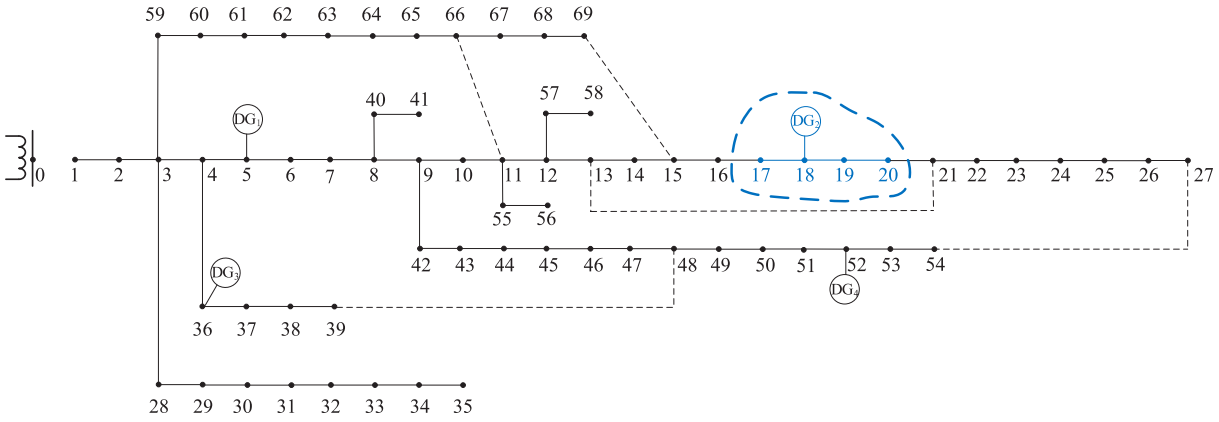

Fig. 5. Island partition with DG_2 as the initial node (in blue). (For interpretation of the references to color in this figure legend, the reader is referred to the web version of this article.)

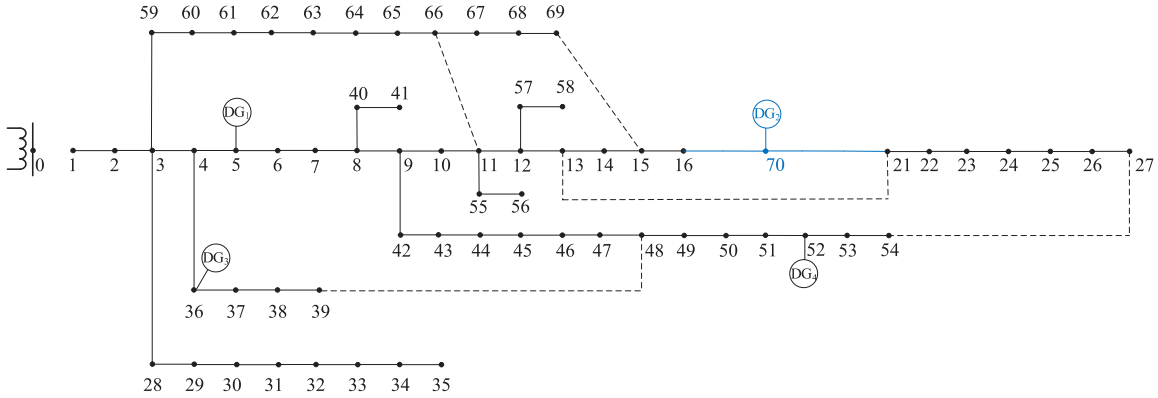

Fig. 6. The topology after s_1 compression.

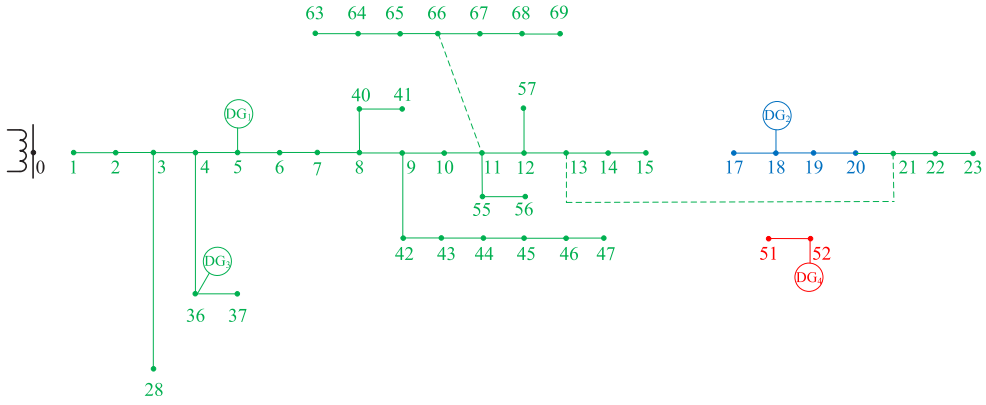

Fig. 7. Island partition scheme at 2627_{th} h.

load points contained in compression nodes 71 and 72 can be restored by DG at this moment, including {1∼15, 17∼23, 28, 36∼37, 40∼47, 51∼52, 55∼57, 63∼69}. According to figure $\boldsymbol{G}'$, the compressed nodes 71 and 72 are restored to obtain the island partition scheme with a ring network. To ensure the radial constraint of DN, the Prim algorithm based on the minimum spanning tree breaks the corresponding branches with higher weights. Disconnect the interconnection switch 15–69 to obtain the final island partition scheme, as shown in Fig. 7.

In order to demonstrate the innovation and effectiveness of the proposed method, the flexibility of interconnection switch is considered in the island partition model is analyzed. In addition, calculation speed and island benefit of the proposed method are compared with the common intelligent algorithm. It is found that the integration of interconnection switch makes a significant effect on island benefit and the computing speed of island partition is significantly improved under the premise of island benefit. The comparation result is shown in Table 3.

The fault lasts for 4 h. The island partition scheme at another three moments is shown in Figs. 8–10. The final load node that can be recovered under this fault is {1, 2, 3, 4, 5, 6, 7, 12, 13, 14, 15, 18, 19, 20, 21, 22, 23, 28, 36, 52, 57}. The final island partition scheme under this fault is shown in Fig. 11.

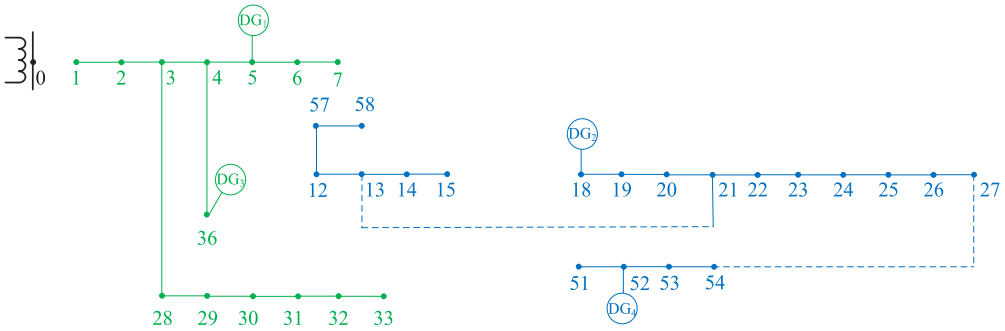

Fig. 8. Island partition scheme at 2624_{th} h.

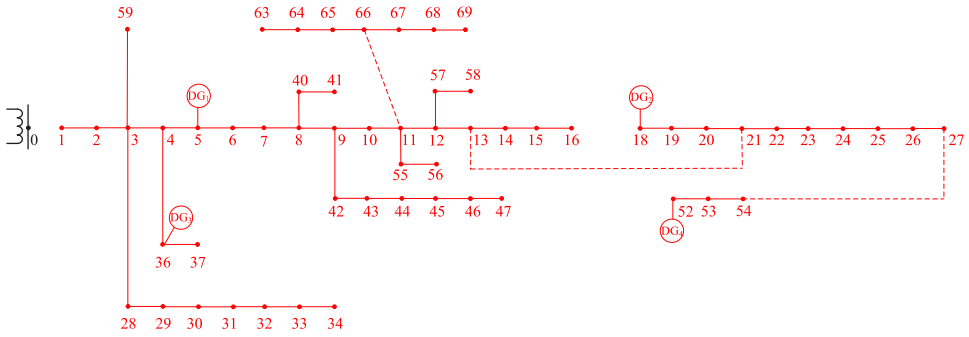

Fig. 9. Island partition scheme at 2625_{th} h.

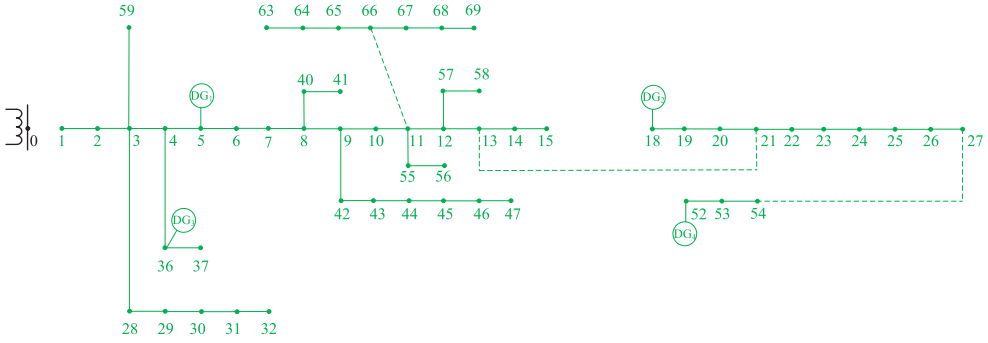

Fig. 10. Island partition scheme at 2626_{th} h.

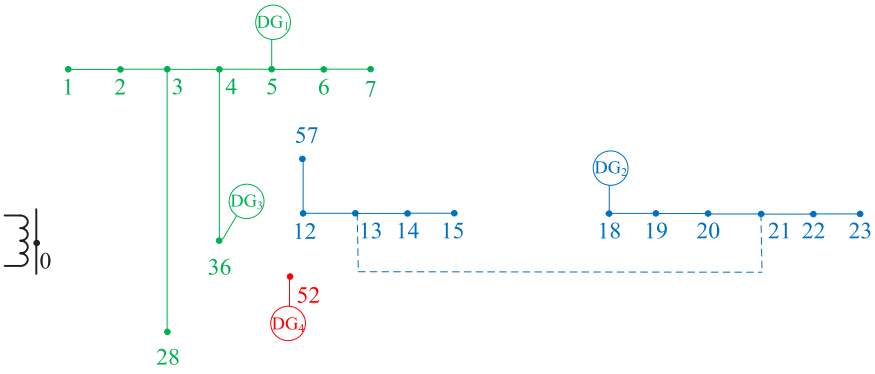

Fig. 11. The final island partition scheme during the fault period (2624 h–2627 h).

4.3. CC evaluation results

4.3.1. CC calculation results based on different reliability indices

To measure the impact of different reliability indices on DG CC, the EENS and average service availability index S_E are selected as reliability indices to evaluate DG CC. The search process of selecting the EENS as the reliability index is shown in Fig. 12. The EENS before DG integration is 2.466×10^5 kWh and the value is regarded as the reliability benchmark. The power supply reliability is improved after the integration of 6 MW DG, and

Table 3
Comparison of island benefits under different methods at 2627th hour.

	Calculation speed/s	Island benefit
Proposed method (with interconnection switch)	0.32	27 648.18
Proposed method (without interconnection switch)	0.34	23 482.25
Genetic algorithm (Wu et al., 2015)	5.71	27 390.31
Particle swarm optimization (Hosseinnezhad et al., 2018)	67.50	26 042.78

Table 4
The CC search results based on different reliability indices.

	ΔP_L/kW	EENS/kWh		ΔP_L/kW	S_E/%
1st search	1901.2	319 629.4	1st search	1901.2	99.808
2nd search	950.6	262 199.5	2nd search	950.6	99.857
3rd search	475.3	235 255.5	3rd search	475.3	99.921
4th search	712.5	241 192.4	4th search	712.5	99.906
5th search	831.8	251 037.1	5th search	831.8	99.872
6th search	772.7	248 224.3	6th search	743.0	99.880
7th search	772.7	246 467.1			

Fig. 12. The CC search results based on EENS.

the EENS index is reduced to 1.328×10^5 kWh. Continuously adjusting the load level based on dichotomy, the search process stops when the difference between the two reliability indices is less than a set minimum value. The search process of selecting S_E as the reliability index is shown in Fig. 13. The average service availability index S_E before DG integration is 99.879%. After the integration of DG, the load level is continuously adjusted based on the dichotomy. The CC calculation is of convergence when the average service availability index S_E reaches 99.880%. The CC calculation results of each iteration are shown in Table 4. The evaluation results of DG CC based on different reliability indices are found to be different. In addition, artificially selecting a minimum value as the convergence criteria requires 6–7 iterations or even longer, which takes up a considerable amount of calculation time.

4.3.2. The CC search results based on hypothesis testing

The reliability calculation results based on SMCS are random and the final result of CC searching is determined by hypothesis testing. The significance level of the hypothesis test is set as $\alpha = 0.05$. Independently obtain a sample of reliability level from the population X_1 with sampling times n_1 of 10 000, and calculate the mean value $\overline{X}_1$ and variance S_1^2 of the sample. Adjust the load level based on dichotomy. Obtain a sample of reliability level from the population X_2 with sampling times n_2 of 1000, and calculate the mean value $\overline{X}_2$ and variance S_2^2 of the sample. The CC calculation process converges until Hypothesis H_0 is satisfied.

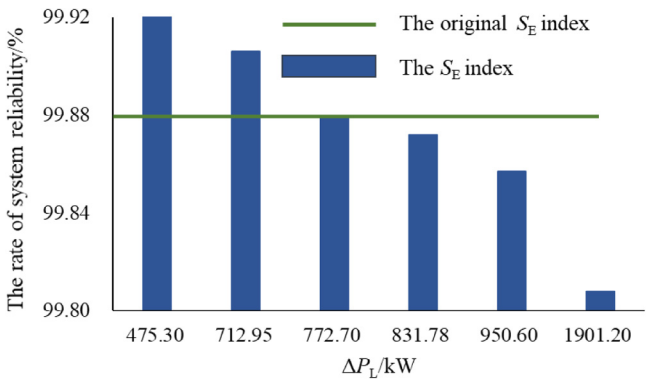

Fig. 13. The CC search results based on S_E.

After calculation, the mean value $\overline{X}_1$ of samples by population X_1 is 20 153.2 kWh, and the variance S_1^2 is 4.15×10^8 kWh ^{2}. When the load level increases by 712.5 kWh, the mean value $\overline{X}_2$ of samples by population X_2 is 20 153.2 kWh, and the variance S_2^2 is 4.15×10^8 kWh ^{2}. At this time, the hypothesis of H_0 is met and no significant difference between two population is considered. The CC of the 6 MW DG is 712.5 kW. The comparison of samples extracted from the two populations is shown in Fig. 14. The reliability indices of samples taken from the two populations are arranged in ascending order. Population X_1, the p_{th} percentile ($p = 1, 2 \ldots 100$) of the sampling is taken as the abscissa. Population X_2, the p_{th} percentile of the sampling, is taken as the ordinate. Fitting the change trend of the sampling point, the fitting curve is found to be similar to the $y = x$ function curve, showing that the distribution of the reliability evaluation results of the two populations is basically the same. The CC search process based on the hypothesis test is shown in Fig. 15. The green box shows the reliability level before DG integration. After four iterative calculations, the reliability level is shown as the blue box. The quartile, median and third quartile of the blue box are very close to the original green box, which satisfies the Hypothesis H_0.

If the convergence criteria of CC searching are an artificially selected minimum value, improper selection may have a great impact on the number of iterations and calculation speed. Next, the evaluation results using the minimum value as the convergence criteria are compared with the evaluation results based on the hypothesis test, as shown in Fig. 16. After four iterative calculations, the method based on the hypothesis test obtained a DG CC evaluation result of 712.5 kW. Based on the minimum value criteria, the DG CC evaluation result obtained after 7 searches is 743.0 kW, and the difference between the two methods is only 4.1%. Therefore, the CC search method based on hypothesis testing can overcome the difficulty of convergence caused by the artificial selection of convergence criteria. The evaluation speed and convergence accuracy are fully considered in this method.

4.3.3. Marginal CC rate

The evaluation results of the CC, CC rate and marginal CC rate under different installed capacity of DG are given in Table 5. The CC evaluation result is 59.43 kW when DG_1(1 MW PV equipment) is integrated into DN, and the marginal CC rate of DG_1 is 5.94%. The CC evaluation result is 416.06 kW after the integration of DG_2 (2 MW wind turbine) and the marginal CC rate of DG_2 is 17.83%. Then, DG_3 (1 MW PV equipment) is integrated into the DN. The CC value of the 4 MW DG is increased to 468.08 kW, but the marginal CC of the 1 MW PV is only 5.20%. Finally, the CC evaluation result is 743.01 kW after the integration of DG_4(2 MW wind turbine), and the marginal CC rate of DG_4 is 12.38%. The calculation results are shown in Fig. 17. The different DG penetration

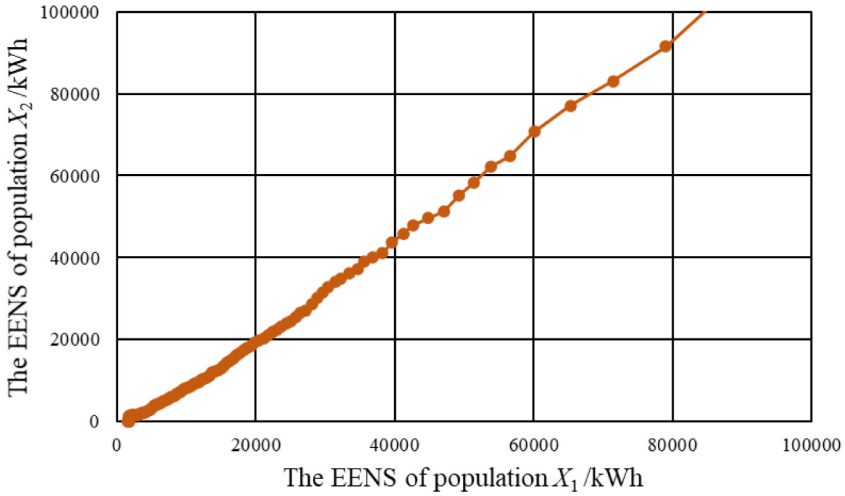

Fig. 14. Reliability level of samples extracted from two populations.

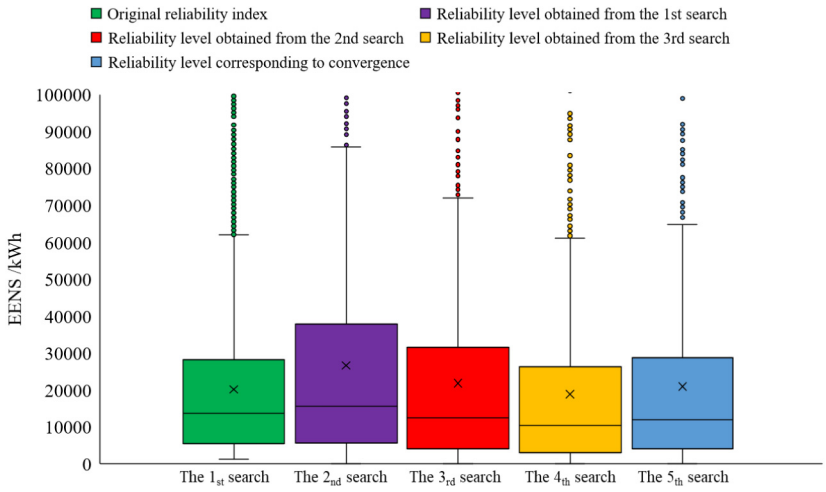

Fig. 15. Box diagram of the reliability level of samples extracted from two populations. (For interpretation of the references to color in this figure legend, the reader is referred to the web version of this article.)

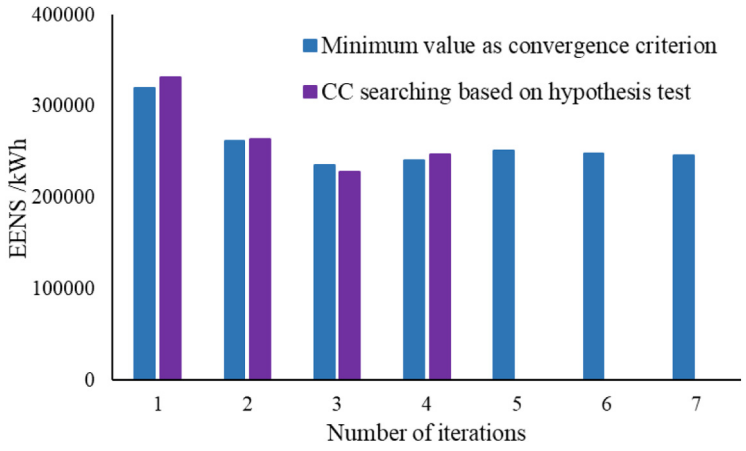

Fig. 16. Comparison of the CC search process under different methods.

levels and type of renewable energy generation are easily found to have a significant impact on the DG CC. With the increase in DG penetration levels, the CC value is improved as well. This is because with the increase of DG installed capacity, the power supply recovery potential of DG under fault state is gradually improved. Therefore, the reliability level and the equivalent load carrying capacity increase as well. However, the CC rate decreases obviously because the utilization rate of DG decreases along with the increase of DG penetration level. In addition, the overall CC rate varies alternatively after the integration of different type of

Table 5
DG CC result under different installed capacity.

The capacity of DG	ELCC/kW	CC rate r_c	Marginal CC/kW	Marginal CC rate
6 MW (4 MW wind turbine + 2 MW PV)	743.01	12.38%	274.93	13.75%
4 MW (2 MW wind turbine + 2 MW PV)	468.08	11.70%	52.02	5.20%
3 MW (2 MW wind turbine + 1 MW PV)	416.06	13.87%	356.63	17.83%
1 MW (1 MW PV)	59.43	5.94%	59.43	5.94%

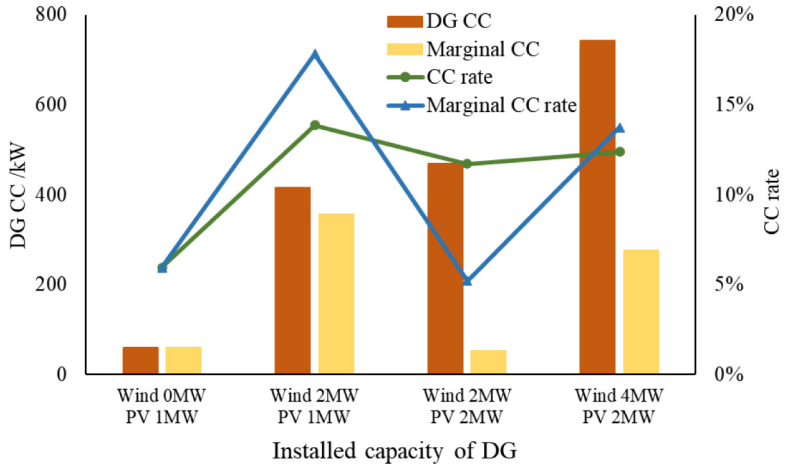

Fig. 17. Variation trend of DG CC under different installed capacity.

DG. Due to the high annual utilization hours of wind turbines, the marginal CC rate of wind turbine is higher than the marginal CC rate of PV equipment. Therefore, the overall CC rate will decrease after the integration of PV equipment, while the effect of wind turbine integration is opposite.

4.3.4. The key factors affecting DG CC

To evaluate the effect of key factors on DG CC, a relevant assessment based on different scenarios is carried out and EENS is used as reliability index. Scenario I is regarded as the control group. The scenario settings are listed in Table 6, and the evaluation results are shown in Fig. 18. According to the evaluation results, the following can be found.

(1) Through the comparison between scenarios I and II, the island partition strategy has a significant impact on DG CC. The difference between the evaluation results under the two scenarios is 64%. The island partition scheme at each moment can be reformulated without considering the constraint of secondary outage, and the power supply restoration potential of DG can be fully utilized under fault state. Compared with the original scenario, the EENS index is greatly reduced, and the power supply reliability is improved, so DG CC can also be significantly improved.

(2) To analyze the impact of load uniformity on DG CC, scenario III evenly distributes the original 3.8 MW load of the 69-bus system, and the load demand of each node is 55.11 kW. The CC evaluation results are similar to those in scenario I, with a difference of only 1%. The comparison results show that the load uniformity has little effect on DG CC.

(3) The evaluation of DG CC under different failure rates is carried out in scenarios I, IV and V, and the obtained CC results are also relatively close. The maximum difference between the three scenarios is no more than 8%, indicating that the failure rate of system components is not a key factor affecting DG CC.

(4) To assess the impact of DG integration location on CC, change the original DG integration node {5, 18, 36, 52} into node {11, 21, 27, 48}. The new integration location is closer to the interconnection switch and the searching path is more extensive. The DG CC under scene VI and scene I found to be very close, and the difference between them is only 1%. The results show that the integration location of the DG is not the decisive factor in determining the CC value.

(5) The CC evaluation of the 6 MW DG on the Institute of Electrical and Electronics Engineers (IEEE) 33-bus system is carried out under scenarios VII and VIII. The detailed parameters of the IEEE 33 bus system can be seen in the appendix. When the secondary outage constraint is not considered, the CC calculation results under the two scenarios differ by 42%. When the secondary outage constraint is considered, the CC calculation results under the two scenarios differ by 52%. It is not difficult to find that DN topology has an important impact on the CC calculation results.

In summary, the DN topology and island partition strategy have a significant impact on DG CC, while load uniformity, failure rate and DG integration location are not key factors affecting DG CC. It should be noted that the convergence speed of sequential Monte Carlo method is less related with the scale of the analyzed system. And, the searching of heuristic prospective greedy algorithm starts from the DG integration node and automatically identifies the adjacent nodes through the connection matrix. The calculation time is basically proportional to the scale of power system. Therefore, the proposed DG CC evaluation method is with good expansibility.

5. Conclusion

A distributed generation (DG) credible capacity (CC) evaluation method based on island partition is proposed in the paper. The power supply restoration potential of DG is fully utilized under fault state. Therefore, the reliability of a distribution network (DN) under random faults can be analyzed accurately by an island partition model, which lays a foundation for DG CC evaluation

Table 6
Parameter settings of each scenario.

Scenario	The capacity of DG/kW	Failure rate/ (times per year)	Whether the load is uniform	Secondary outage constraint	The DG integration node	DG CC rate
I	6000	0.2	no	Considered	5, 18, 36, 52	12.38%
II	6000	0.2	no	Not considered	5, 18, 36, 52	34.18%
III	6000	0.2	yes	Considered	5, 18, 36, 52	12.52%
IV	6000	0.4	no	Considered	5, 18, 36, 52	13.00%
V	6000	0.1	no	Considered	5, 18, 36, 52	12.05%
VI	6000	0.2	no	Considered	11, 21, 27, 48	12.28%
VII	6000	0.2	no	Considered	7, 11, 14, 29	7.23%
VIII	6000	0.2	no	Not considered	7, 11, 14, 29	18.87%

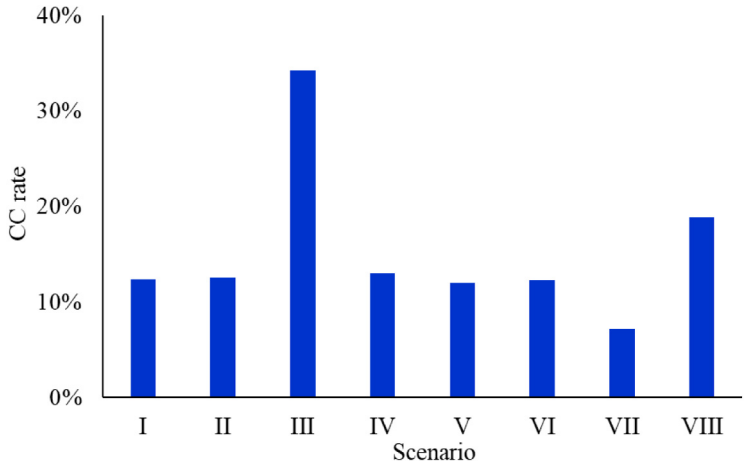

Fig. 18. Evaluation result of DG CC under each scenario evaluation.

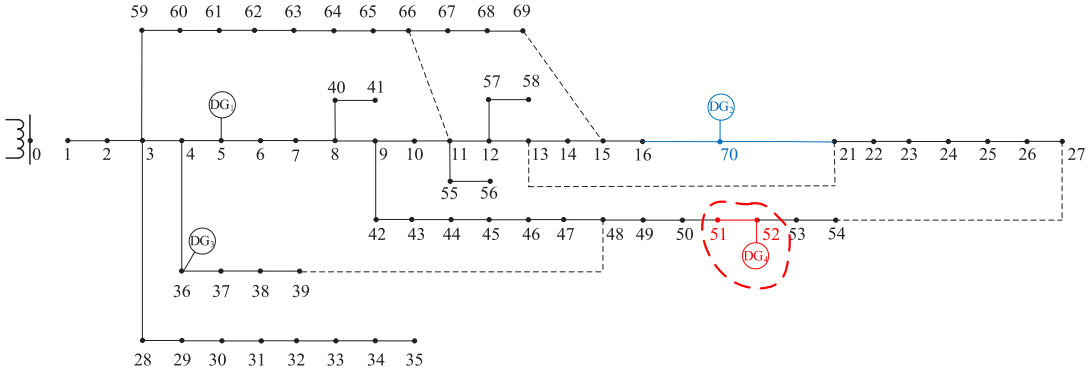

Fig. A.1. Island partition with DG_4 as the initial node (in red). (For interpretation of the references to color in this figure legend, the reader is referred to the web version of this article.)

based on the equal power supply reliability criterion. The characteristic is that the fluctuation of DGs and load, interconnection switch, load priority and secondary outage constraint are fully considered in the island partition model. The island partition model can be solved quickly through the prospective greedy algorithm and Prim algorithm. In the CC search process, the hypothesis test method is used to reconcile the calculation speed and accuracy. Based on the proposed method, case studies of the PG&E 69-bus system are analyzed. According to the evaluation results, it is found that:

(1) The island partition strategy has a significant impact on the DG CC value. When the secondary outage constraint has to be considered, the evaluation result of DG CC is only one third of that without considering the constraint.

(2) The DN topology has a significant impact on the DG CC value. Targeted assessment is necessary for even the same capacity DG in different DN topologies. The CC evaluation results are not universal.

(3) The overall CC value increases with different DG penetration levels, while the CC rate of each DG type decreases gradually. The overall CC rate varies alternatively due to the integration of different type of DG. The CC rate of PV equipment is approximately 5%, while the CC rate of wind turbine is approximately 13% 18%.

(4) The failure rate of system components has little effect on DG CC because the failure rate affects the absolute reliability value, while the evaluation of CC focuses on the relative reliability value under the equal reliability criterion.

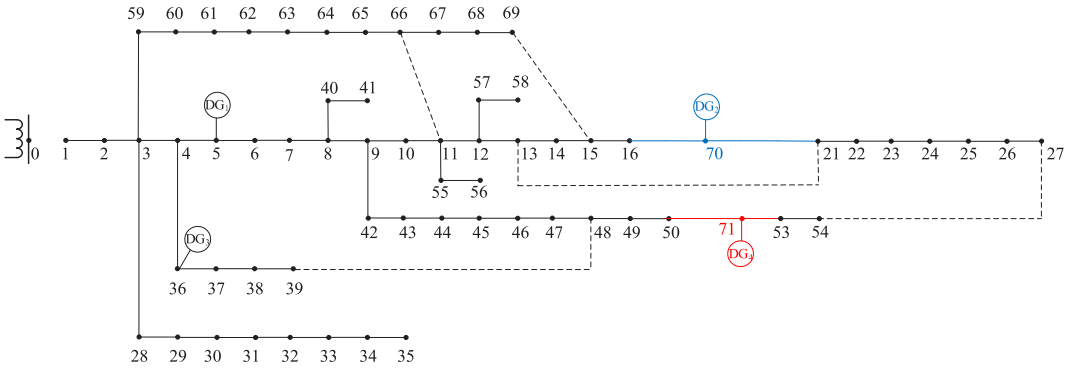

Fig. A.2. Topology after s_2 compression.

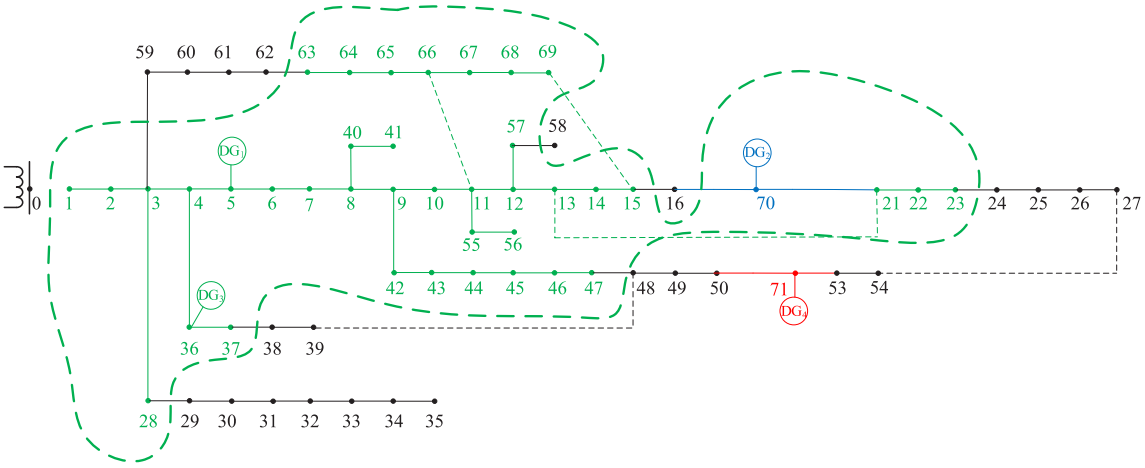

Fig. A.3. Island partition with DG_1 as the initial node (in green). (For interpretation of the references to color in this figure legend, the reader is referred to the web version of this article.)

CRediT authorship contribution statement

Chen Jiahao: Resources, Algorithm. **Sun Bing:** Conceptualization, Methodology. **Li Yunfei:** Software. **Jing Ruipeng:** Translation. **Zeng Yuan:** Supervision. **Li Minghao:** Writing – original draft.

Declaration of competing interest

The authors declare that they have no known competing financial interests or personal relationships that could have appeared to influence the work reported in this paper.

Data availability

No data was used for the research described in the article.

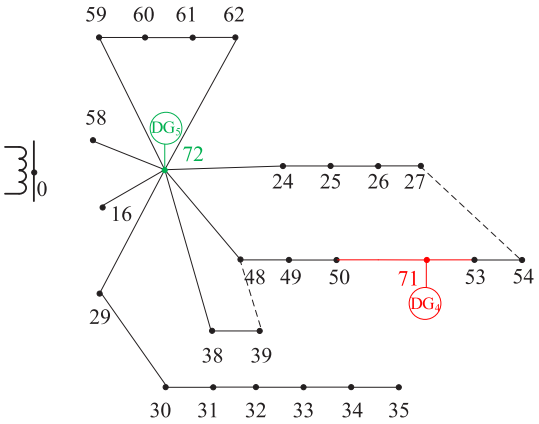

Fig. A.4. Topology after s_3 compression.

Acknowledgments

This work was supported by the State Grid scientific and technological projects of China (SGTYHT/21-JS-223), the fund of Chinese Academy of Engineering Institute Local Cooperation Project (2020HENZDA02), the 67th Postdoctoral Fund and Independent innovation fund of Tianjin University, China in 2021.

Appendix A

When DG_4 is used for power supply recovery, since the DG_4 is integrated into load node 52, it is selected as the initial node of the knapsack problem. Search other load nodes that can be recovered in the neighborhood of the knapsack based on the prospective greedy algorithm until the capacity of DG is insufficient. The power supply restoration scheme of DG_4 is shown in Fig. A.1. The nodes drawn into the backpack are compressed as a new node s_2, the sum load of the island is 33.57 kW, and the benefit value is 33.57. The remaining active power of DG_4 is 95.06 kW. The compressed node number is recorded as node 71, and the topology after s_2 compression is shown in Fig. A.2. After the calculation of a DG is completed, the load node and DGs in its recovery area must be compressed into a node, and the DN topology is updated at the same time. The compressing

Table B.1
Load demand and priority of PG&E 69-bus system.

Node number i	The priority PR_i	Load demand/kVA	Node number i	The priority PR_i	Load demand/kVA
1	10	0	36	10	0
2	10	0	37	100	79+j56.4
3	10	0	38	10	384.70+j274.5
4	1	0	39	10	384.70+j274.5
5	10	0	40	10	40.5+j28.3
6	100	2.6+j2.2	41	10	3.6+j2.7
7	10	40.4+j30	42	10	4.35+j3.5
8	10	75+j54	43	100	26.4+j19
9	10	30+j22	44	10	24+j17.2
10	10	28+j19	45	1	0
11	10	145+j104	46	10	0
12	10	145+j104	47	10	0
13	10	8+j5.5	48	10	100+j72
14	10	8+j5.5	49	10	0
15	10	0	50	1	1244+j888
16	10	45.5+j30	51	1	32+j23
17	1	60+j35	52	10	0
18	10	60+j35	53	100	227+j162
19	100	0	54	100	59+j42
20	10	1+j0.6	55	10	18+j13
21	10	114+j81	56	10	18+j13
22	10	5.3+j3.5	57	10	28+j20
23	10	0	58	10	28+j20
24	10	28+j20	59	10	26+j18.55
25	10	0	60	1	26+j18.55
26	10	14+j10	61	10	0
27	10	14+j10	62	1	24+j17
28	100	26+j18.6	63	10	24+j17
29	10	26+j18.6	64	10	1.2+j1
30	10	0	65	10	0
31	10	0	66	100	6+j4.3
32	100	0	67	10	0
33	1	14+j10	68	10	39.22+j26.3
34	10	19.5+j14	69	100	39.22+j26.3
35	1	6+j4			

Table B.2
Load demand and priority of IEEE 33 bus system.

Node number i	The priority PR_i	Load demand/kVA	Node number i	The priority PR_i	Load demand/kVA
1	100	100+j60	17	1	90+j40
2	100	90+j40	18	10	90+j40
3	10	120+j80	19	1	90+j40
4	10	60+j30	20	1	90+j40
5	100	60+j20	21	1	90+j40
6	10	200+j100	22	10	90+j50
7	100	200+j100	23	1	420+j200
8	10	60+j20	24	1	420+j200
9	1	60+j20	25	10	60+j25
10	10	45+j30	26	1	60+j25
11	100	60+j35	27	1	60+j20
12	10	60+j35	28	10	120+j70
13	10	120+j80	29	100	200+j600
14	100	60+j10	30	10	150+j70
15	10	60+j20	31	100	210+j100
16	1	60+j20	32	10	60+j40

operation lays a foundation to prevent the restored load node from hindering the next island formulation.

When DG_1 is used for power supply recovery, the final scheme of power supply recovery is {1∼15, 21∼23, 28, 36∼37, 40∼47, 55∼57, 63∼69, 70}. The island partition with DG_1 is shown in Fig. A.3. The nodes drawn into the backpack are compressed as a new node s_3, the sum load of island is 1026.92 kW, and the benefit value is 27 190.47. The compressed node number is recorded as node 72, and the topology after s_3 compression is shown in Fig. A.4. Since node 70 is drawn into the island, the load demand and benefit value of the compressed node are also considered in the power supply recovery scheme of DG_1. Then, the island partition scheme of DG_2 and DG_1 is merged. DG_1 restores power for loads 5, 36 and 70 at the same time. The remaining electricity of DG_1, DG_2 and DG_3 must be merged into a new DG. The new DG is recorded as DG_5 and integrated into compression node 72.

Appendix B

See Tables B.1 and B.2.

References

Aghaei, J., Akbari, M., Roosta, A., et al., 2013. Multi objective generation expansion planning considering power system adequacy. Electr. Power Syst. Res. 102, 8–19.

Ahangar, A., Gharehpetian, G., Baghaee, H., 2020. A review on intentional controlled islanding in smart power systems and generalized framework for ICI in microgrids. Int. J. Electr. Power Energy Syst. 118 (1), in press.

Amelin, M., 2009. Comparison of capacity credit calculation methods for conventional power plants and wind power. IEEE Trans. Power Syst. 24 (2), 685–691.
Bethany, F., Wesley, C., Sun, Y., et al., 2017. 8760-Based Method for Representing Variable Generation Capacity Value in Capacity Expansion Models. National Renewable Energy Lab. (NREL), Golden, CO (United States).
Cai, J., Xu, Q., 2021. Capacity credit evaluation of wind energy using a robust secant method incorporating improved importance sampling. Sustain. Energy Technol. Assess. 43, in press.
Chen, F., Li, F., Feng, W., et al., 2019. Reliability assessment method of composite power system with wind farms and its application in capacity credit evaluation of wind farms. Electr. Power Syst. Res. 166, 73–82.
Costa, P., Matos, M., 2010. Capacity credit of microgeneration and microgrids. Energy Policy 38 (10), 6330–6337.
Fang, X., Hu, Q., Bo, R., et al., 2021. Redesigning capacity market to include flexibility via ramp constraints in high-renewable penetrated system. Int. J. Electr. Power Energy Syst. 128, in press.
Hawkes, A., Leach, M., 2008. The capacity credit of micro-combined heat and power. Energy Policy 36 (4), 1457–1469.
Hosseinnezhad, V., Rafiee, M., Ahmadian, M., et al., 2018. Optimal island partitioning of smart distribution systems to improve system restoration under emergency conditions. Int. J. Electr. Power Energy Syst. 97, 155–164.
Li, G., Bie, Z., Xie, H., et al., 2016. Customer satisfaction-based reliability evaluation of active distribution networks. Appl. Energy 162, 1571–1578.
Li, G., Huang, Y., Bie, Z., 2018. Reliability evaluation of smart distribution systems considering load rebound characteristics. IEEE Trans. Sustain. Energy 9 (4), 1713–1721.
Luo, F., Xu, J., Zhang, T., 2021. Quantitative evaluation of power supply reliability improvement in distribution network by customer-side integrated energy system. Energy Rep. 7 (6), 233–241.
Lynch, M., Nolan, S., Devine, M., et al., 2019. The impacts of demand response participation in capacity markets. Appl. Energy 250, 444–451.
Madaeni, S., Sioshansi, R., Denholm, P., 2012. Comparison of Capacity Value Methods for Photovoltaics in the Western United States. National Renewable Energy Lab. (NREL), Golden, CO (United States).
Miao, S., Yang, H., Gu, Y., 2018. A wind vector simulation model and its application to adequacy assessment. Energy 148, 324–340.
Oboudi, M., Hooshm, R., Karamad, A., 2017. A feasible method for controlled intentional islanding in microgrids based on PSO algorithm. Swarm Evol. Comput. 35, 14–25.
Ochoa, L., Dent, C., Harrison, G., 2010. Distribution network capacity assessment: variable DG and active networks. IEEE Trans. Power Syst. 25 (1), 87–95.
Paik, C., Chung, Y., Kim, Y., 2021. ELCC-based capacity credit estimation accounting for uncertainties in capacity factors and its application to solar power in Korea. Renew. Energy 164, 833–841.
Rajam, S., 2020. Effect of demand response program of loads in cost optimization of microgrid considering uncertain parameters in PV/WT, market price and load demand. Energy 194, in press.
Remiorz, L., Kotowicz, J., Uchman, W., 2018. Comparative assessment of the effectiveness of a free-piston stirling engine-based micro-cogeneration unit and a heat pump. Energy 148, 134–147.
Ryan, L., Dillon, J., Monaca, S., et al., 2016. Assessing the system and investor value of utility-scale solar PV. Renew. Sustain. Energy Rev. 64, 506–517.
Salama, H., Said, S., Aly, M., et al., 2021. Studying impacts of electric vehicle functionalities in wind energy-powered utility grids with energy storage device. IEEE Access 9, 45754–45769.
Shahidirad, N., Niroom, M., Hooshm, R., 2018. Investigation of PV power plant structures based on Monte Carlo reliability and economic analysis. IEEE J. Photovolt. 8 (3), 1–9.
Slota, J., Root, J., Devine, K., et al., 2020. Scalable, multi-constraint, complex-objective graph partitioning. IEEE Trans. Parallel Distrib. Syst. 31 (12), 2789–2801.
Sun, B., Li, Y., Zeng, Y., et al., 2021. The total social cost evaluation of two wind and PV energy development modes: A study on henan of China. Energy Rep. 7, 6565–6580.
Sun, B., Li, Y., Zeng, Y., et al., 2022. Optimization planning method of distributed generation based on steady-state security region of distribution network. Energy Rep. 8, 4209–4222.
Sun, B., Yu, Y., Qin, C., 2017. Should China focus on the distributed development of wind and solar photovoltaic power generation? A comparative study. Appl. Energy 185, 421–439.
Voorspools, K., d'Haeseleer, W., 2006. An analytical formula for the capacity credit of wind power. Renew. Energy 31 (1), 45–54.
Wang, H., Zhao, J., Sun, Q., et al., 2019. Probability modeling for PV array output interval and its application in fault diagnosis. Energy 189, in press.
Wen, J., Yang, J., Wang, T., 2021. Path planning for autonomous underwater vehicles under the influence of ocean currents based on a fusion heuristic algorithm. IEEE Trans. Veh. Technol. 70 (9), 8529–8544.
Wilton, E., Delarue, E., D'Haeseleer, W., et al., 2014. Reconsidering the capacity credit of wind power: application of cumulative prospect theory. Renew. Energy 68, 752–760.
Wu, Y., Tang, Y., Han, B., et al., 2015. A topology analysis and genetic algorithm combined approach for power network intentional islanding. Int. J. Electr. Power Energy Syst. 71, 174–183.
Zeng, B., Wei, X., Zhao, D., et al., 2018. Hybrid probabilistic-possibilistic approach for capacity credit evaluation of demand response considering both exogenous and endogenous uncertainties. Appl. Energy 229, 186–200.
Zhang, N., Kang, C., Xiao, J., et al., 2015. Review and prospect of wind power capacity credit. Proc. Chin. Soc. Electr. Eng. 35 (1), 82–94.
Zhang, B., Wang, M., Su, W., 2021. Reliability analysis of power systems integrated with high-penetration of power converters. IEEE Trans. Power Syst. 36 (3), 1998–2009.
Zhao, J., Oh, U., Choi, J., 2019a. Power system reliability evaluation including capacity credit considering wind energy with energy storage systems in China. IFAC-Papers Online 52 (4), 348–353.
Zhao, E., Song, J., Chen, J., et al., 2021. Will auctioning promote the renewable energy generation in China? Adv. Clim. Change Res. 13 (1), 107–117.
Zhao, J., Zhang, M., Yu, H., et al., 2019b. An islanding partition method of active distribution networks based on chance-constrained programming. Appl. Energy 242, 78–91.
Zhou, E., Cole, W., Frew, B., 2018. Valuing variable renewable energy for peak demand requirements. Energy 165, 499–511.
Zhou, Y., Marcarelli, P., Mutale, J., 2016. Framework for capacity credit assessment of electrical energy storage and demand response. IET Gener. Transm. Distrib. 10 (9), 2267–2276.